Plumbene layer grown on Si(111)$\sqrt{3} \times \sqrt{3}$-B and its restructuring by Mg adsorption

A. N. Mihalyuk [1,2] L. V. Bondarenko [1] A. Y. Tupchaya,[1] Y. E. Vekovshinin [1] N. V. Denisov [1]
D. V. Gruznev [1] A. V. Zotov [1] and A. A. Saranin [1,*]

[1]*Institute of Automation and Control Processes, FEB RAS, 690041 Vladivostok, Russia*

[2]*Institute of High Technologies and Advanced Materials, Far Eastern Federal University, 690950 Vladivostok, Russia*

(Received 11 September 2024; revised 2 February 2025; accepted 19 February 2025; published 3 March 2025)

Using scanning tunneling microscopy observations, the Si(111)$\sqrt{3} \times \sqrt{3}$-B surface was experimentally proved to be a suitable substrate for hosting high-buckled plumbene. Magnesium (Mg) adsorbed onto the grown plumbene intercalates between the Pb layer and Si(111)$\sqrt{3} \times \sqrt{3}$-B substrate to form the Pb/Mg/Si(111):B atomic sandwich. Meanwhile, the Pb layer undergoes significant transformations: its original coverage of 2.0 monolayers (ML) reduces to 1.33 ML of Pb, as revealed via the density functional theory (DFT) *ab initio* random structure search analysis. The layer is arranged in a striped 3×1 structure, which, together with the substrate, adopts the overall 3×3 periodicity. DFT analysis of the band structures of the grown Pb layers revealed that they might possess unique electronic properties. However, the intrinsic properties of the layers appear to be overshadowed by the electronic properties of the real Si(111):B substrate, which underwent a strong subsurface *p*-type doping. The dominated contribution of the substrate bands to the electronic properties was confirmed in the *in situ* low-temperature transport measurements, which showed that the Si(111):B substrate with and without plumbene, as well as Pb/Mg/Si(111):B samples, display very similar conductivity values. The obtained results demonstrate that, while considering possible applications, the substrate hosting the prospective low-dimensional structures (e.g., two-dimensional Xenes) must meet not only the structural but also the electronic requirements.

DOI: 10.1103/PhysRevB.111.125401

I. INTRODUCTION

Among a variety of the low-dimensional materials, those whose thickness approaches the atomic-scale limit are of special interest. The lead (Pb) atomic layers present vivid examples due, at least, to four reasons associated with their advanced properties. First, Pb layer formation on Si(111) was recognized to involve anomalous ultrafast mass transport [1–5]. Second, the Pb monolayers grown on the Ge(111) surface were reported to exhibit a giant Rashba-type spin splitting of the metallic surface-state bands [6–8]. Third, Pb was found to be the only elemental metal, which remains a superconductor down to a single-atom thickness, as in the case of the Pb/Si(111) system, which has become a prototype system for exploring two-dimensional (2D) superconductivity at the atomic-scale limit [9–18]. The fourth reason is associated with the current growing interest in the so-called 2D-Xenes, atomic layers having a graphenelike honeycomb structure [19–22], with plumbene built of Pb atoms being a member of the 2D-Xenes family [23–31]. In addition to a number of theoretical studies on the structural and electronic properties of plumbene [23–27], up to now there have been three experimental studies reporting its successful synthesis on the various substrates, including the $Pd_{1-x}Pb_x$(111) alloy surface [28], the Ir(111) surface covered by Fe monolayer [29], and the Si(111)$\sqrt{3} \times \sqrt{3}$-B surface [30].

Summarizing the reported data, one can see that depending on the hosting substrates, Pb atomic layers adopt various structures and exhibit a variety of electronic properties, for example showing up as a superconductor in the Pb/Si(111) system [9,10] and as a normal metal in the Pb/Ge(111) system [32,33]. In the case of plumbene, its electronic properties might vary in a wide range from insulating [25] to metallic [24] and superconducting [34], depending on the strain, which, in turn, can be affected by the interaction with the hosting substrate. Therefore, forcible alternation of the Pb atomic layer structure, in particular, via modification of the material system incorporating the layer, shows promise for exploring the main regularities controlling the Pb layer structural and electronic properties.

In the present paper, we report on the modifications of the plumbene layer grown on the Si(111)$\sqrt{3} \times \sqrt{3}$-B surface induced by Mg adsorption. The study was partially motivated by the recently reported finding that intercalation of Mg atoms between the double-layer $\sqrt{7} \times \sqrt{3}$-In phase and Si(111) substrate produces a nearly free-standing double-layer In metal, preserving its original structure [35]. However, this is not a general rule, as in the cases of Tl/Si(111) [36] and Pb/Si(111) [37] systems, the structure of the metal layers changes upon Mg intercalation. The set of experimental techniques used in this study includes low-energy electron diffraction, scanning tunneling microscopy, and *in situ* electronic transport measurements using the four-point-probe technique. It was found that adsorbed Mg penetrates beneath the Pb layer to form the Pb/Mg/Si(111):B atomic sandwich, displaying 3×3 surface periodicity. The Pb layer in a sandwich was found to have a

*Contact author: saranin@iacp.dvo.ru

striped structure built of 1.33 ML of Pb. The transport measurements showed that the Si(111)$\sqrt{3} \times \sqrt{3}$-B substrate with and without plumbene, as well as Pb/Mg/Si(111):B samples, display very similar sheet resistance values. The problem was resolved with DFT analysis of the electronic band structures of the systems explored in the present experiments.

II. EXPERIMENTAL AND COMPUTATIONAL DETAILS

Depending on the task, the experiments were performed in one of the two ultrahigh-vacuum systems, including Omicron MULTIPROBE and UNISOKU USM 1500 LT systems. The Omicron MULTIPROBE system equipped with low-energy electron diffraction (LEED), scanning tunneling microscopy (STM), and angle-resolved photoelectron spectroscopy (ARPES) facilities was used to explore the atomic structures of the sample surfaces, as well as to optimize preparation procedures for the formation of the desired surface structures with the best structural quality. Using the adopted preparation procedures, the corresponding structures were reproduced in the UNISOKU USM 1500 LT system, where the *in situ* transport measurements were conducted with the four-point-probe (4PP) technique down to the lowest temperature of about 2 K with an accuracy of the temperature measurements being about 0.1 K. The probes used were gold wires 0.1 mm in diameter, equally spaced by 0.2 mm along a straight line. The system enables us to apply a magnetic field up to 8 T perpendicular to the sample surface. STM images were acquired using Omicron variable-temperature STM-XA operating in a constant-current mode. Mechanically cut PtIr tips were used as STM probes after annealing in vacuum.

Atomically clean Si(111)7 × 7 surfaces were prepared *in situ* by flashing to 1280 °C after the samples were first outgassed at 600 °C for several hours. Pb and Mg were deposited from the tantalum tubes, and B_2O_3 was deposited from the tungsten-wire evaporator. Pb and Mg deposition rates (0.06 and 0.2 ML/min, respectively) were calibrated using STM observations of the Si(111)1 × 1-Pb reconstruction with 1.2 ML of Pb and Si(111)3 × 1-Mg reconstruction with 1/3 ML of Mg, respectively.

Density functional theory (DFT) calculations were performed using the Vienna Ab initio Simulation Package (VASP) [38,39], with core electrons represented by projector augmented wave (PAW) potentials [39,40]. The generalized gradient approximation of Perdew, Burke, and Ernzerhof (GGA-PBE) [41] to the exchange-correlation functional was employed for structure relaxation. To simulate the Pb structures on Si(111)-B surface, we used a slab consisting of four bilayers (BLs) of the substrate with the PBE-optimized bulk Si lattice constant. Hydrogen atoms were used to passivate the Si dangling bonds at the bottom of the slab. The atomic positions of Pb, Mg atoms, and atoms of Si layers within the two BLs of the slab were optimized. The geometry optimization was performed until the residual forces on atoms became smaller than 10 meV/Å. The 7 × 7 × 1 and 5 × 5 × 1 k-point mesh was used to sample the Pb/Si(111)$\sqrt{3} \times \sqrt{3}$-B and (Pb, Mg)/Si(111)-3 × 3-B surface Brillouin zones, respectively. For getting an accurate Si band gap, we applied the DFT-1/2 self-energy correction method [42,43]. The scalar relativistic effects and the spin-orbit coupling (SOC) were taken into account for calculating the band structure. To find the most stable Pb and Pb-Mg structures on the Si(111)-B surface, we used the *ab initio* random structure searching (AIRSS) approach [44,45]. For simulation of the STM images, the Tersoff-Hamann approach [46] was employed.

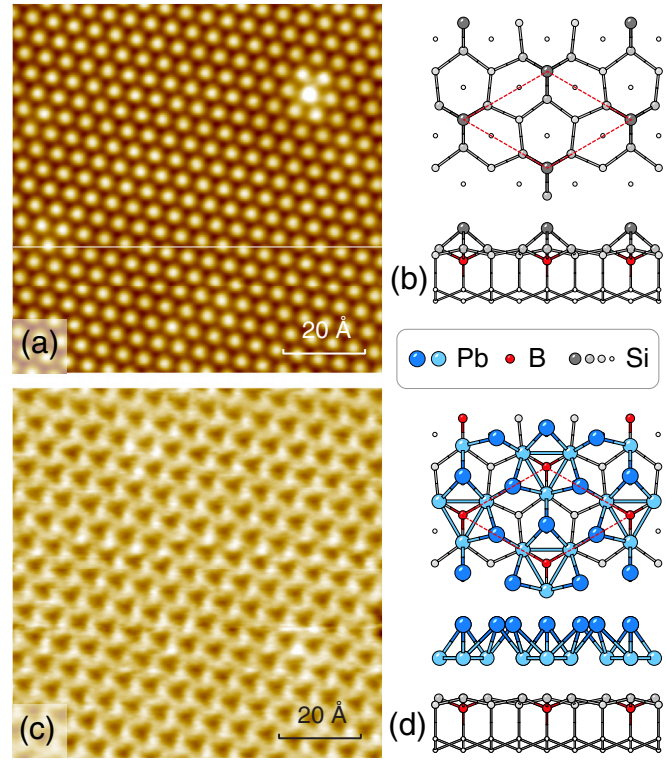

FIG. 1. (a), (c) STM images (90 × 90 Å^2) and (b), (d) corresponding structural models (top and side views) of the bare Si(111)$\sqrt{3} \times \sqrt{3}$-B surface and the plumbene layer grown on it, respectively. STM images were acquired at (a) +1.5 and (c) −0.5 V sample bias. Si atoms in the structural models are shown by the gray balls, B atoms by the red balls, and Pb atoms by the blue balls, with the upper Pb atoms being highlighted by the darker contrast. The $\sqrt{3} \times \sqrt{3}$ unit cells are outlined by the rhombuses.

III. RESULTS AND DISCUSSION

A. Formation and atomic structures

For the formation of the plumbene layer on the Si(111)$\sqrt{3} \times \sqrt{3}$-B surface, we employed the basic preparation procedure, which had been used in our previous work [30]. As a first step, the Si(111)$\sqrt{3} \times \sqrt{3}$-B surface was prepared using one of the two possible techniques. The first one utilized boron segregation to the surface during high-temperature (∼1000 °C) annealing of the heavily B-doped Si(111) samples with a resistivity of 0.005 Ω cm. In the other technique, the decomposition of B_2O_3 deposited from the tungsten wire evaporator onto the Si(111) surface held at ∼850 °C was employed. In the latter case, n-type Si(111) samples with 20–100 Ohm cm resistivity were used. Under appropriate precautions, both techniques ensured the preparation of a homogeneous Si(111)$\sqrt{3} \times \sqrt{3}$-B surface with a modest density of surface defects [Fig. 1(a)]. Recall that the Si(111)$\sqrt{3} \times \sqrt{3}$-B surface incorporates 1/3 ML of B atoms

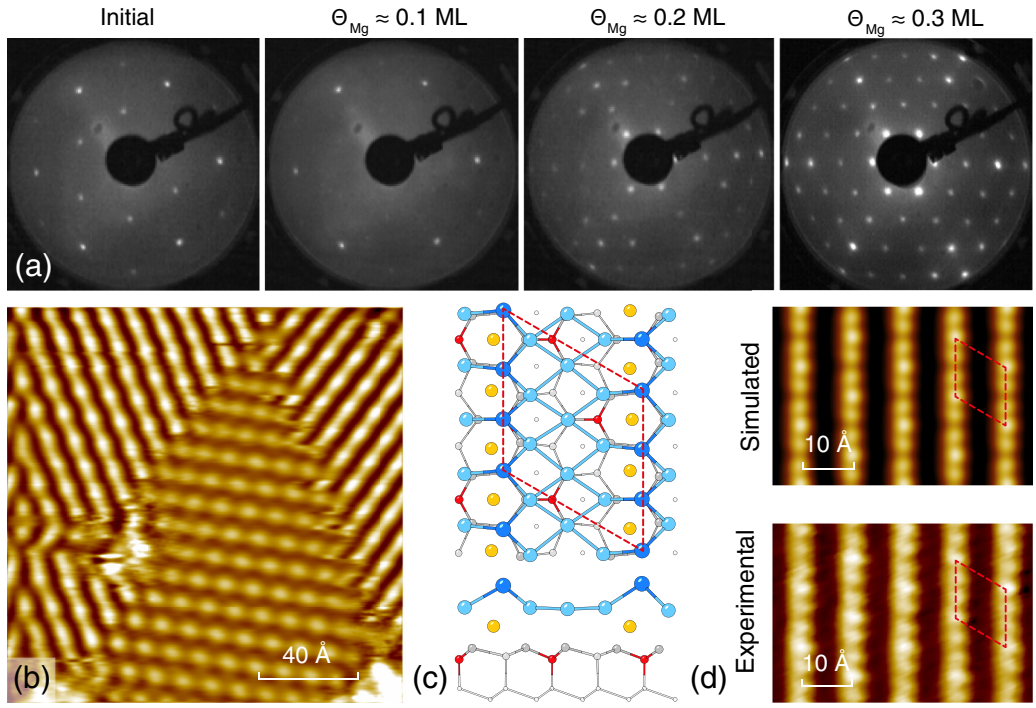

FIG. 2. (a) Set of LEED patterns ($E_p = 54$ eV) illustrating evolution of the surface structure after adsorption of 0.1, 0.2, and 0.3 ML of Mg onto the Pb/Si(111) : B-$\sqrt{3} \times \sqrt{3}$ surface. (b) Filled-state (−0.1 V) 160 × 160 Å^2 STM image of the Pb/Mg/Si(111) : B-3 × 3 surface occurring in the three domain orientations. (c) Structural model of the 3 × 3-(Pb, Mg)/Si(111) : B surface, where Si atoms are shown by the gray balls, B atoms by the red balls, Mg atoms by the yellow balls, and Pb atoms by the blue balls, with the upper Pb atoms being highlighted by the darker contrast. (d) Simulated (upper panel) and experimental (lower panel) STM images of the Pb/Mg/Si(111) : B-3 × 3 surface acquired at a sample bias of +0.01 V. The 3 × 3 unit cells are indicated in (c) and (d) by the red rhombuses.

substituted for Si atoms in the so-called S_5 sites in the top Si(111) bilayer and 1/3 ML of Si adatoms occupying the T_4 sites directly above B atoms [47–49] [Fig. 1(b)].

At the next step, approximately 2.0 ML of Pb was deposited onto the Si(111)$\sqrt{3} \times \sqrt{3}$-B surface held at room temperature (RT) followed by annealing at ∼200 °C for 20 s, resulting in the formation of the ordered Pb layer preserving the $\sqrt{3} \times \sqrt{3}$ periodicity [Fig. 1(c)]. The Pb layer was reported [30] to incorporate a Pb bilayer arranged in the slightly distorted honeycomb lattice (i.e., having essentially the structure of the *high-buckled plumbene*), while the B atoms remain in their original positions in the S_5 sites in contrast to the Si adatoms, which are removed from the structure [Fig. 1(d)].

Then magnesium was deposited onto the prepared plumbene layer at RT. Upon Mg deposition, the initial $\sqrt{3} \times \sqrt{3}$ LEED pattern changes to the apparent 1 × 1 one at about 0.1 ML Mg coverage, then to the LEED pattern, which looks like that of the three-domain 3 × 1 structure at 0.2 ML of Mg, and eventually evolves to the well-defined sharp and bright 3 × 3 LEED pattern at about 0.3 ML of Mg [Fig. 2(a)]. High-resolution STM observations reveal that the 3 × 3-(Pb, Mg) surface has a striped structure and occurs in the three possible orientations [Fig. 2(b)]. The stripes are rows of round protrusions with the 1a spacing in the row and the 3a inter-row separation, where $a = 3.84$ Å, the lattice constant of the unreconstructed Si(111)1 × 1 surface. Within the row, every third protrusion is slightly brighter than the others. The mutual ordering of the bright protrusions in the neighboring rows is responsible for the overall 3 × 3 periodicity of the (Pb, Mg)/Si(111):B surface [Fig. 2(d)]. Note that the resulting 3 × 3 unit cell is still anisotropic and has three rotational domains.

To elucidate the atomic structure of the Pb-Mg layer, we employed DFT calculations in the framework of the AIRSS technique. The implementation of the AIRSS approach was as follows. The Pb and Mg atoms were randomly placed onto the 3 × 3 cell of the Si(111):B substrate, and the system was allowed to relax until a local minimum. The procedure was repeated, and the final structures were ranked according to their formation energies. The greater the number of attempts, the higher the probability that the lowest-energy configuration corresponds to the global minimum. In the present study, the number of attempts amounted to about 300 for each Pb content.

The Mg coverage was fixed at 0.33 ML (i.e., 3 Mg atoms per 3 × 3 unit cell), while Pb coverage was varied in the range from 1.0 to 2.0 ML (from 9 to 18 Pb atoms per 3 × 3 unit cell). The system formation energy E_{form} was calculated using the standard thermodynamical expression for the systems with the varied number of atoms [50]:

$$E_{\text{form}} = [E_{\text{slab}} - E_{\text{Si(111):B}} - N_{\text{Pb}}\mu_{\text{Pb}} - N_{\text{Mg}}\mu_{\text{Mg}}]/9,$$

where E_{slab} is the total energy of the Pb/Mg/Si(111):B structure, $E_{\text{Si(111):B}}$ is the energy of the corresponding Si(111):B slab, N_{Pb} and N_{Mg} are the number of Pb and Mg atoms, respectively, and μ_{Pb} and μ_{Mg} are chemical potentials of the appropriate bulk phases. The formation energy is normalized to a single (1 × 1) unit cell.

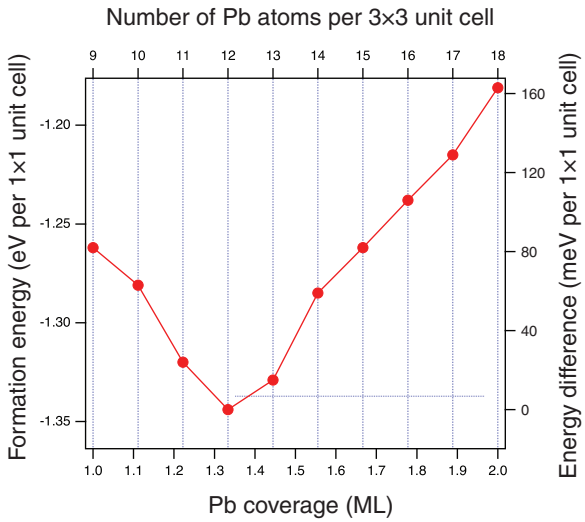

FIG. 3. Dependence of the Pb/Mg/Si(111) : B-3 × 3 structure formation energy on the Pb content, as determined in the DFT calculations in the framework of the AIRSS technique.

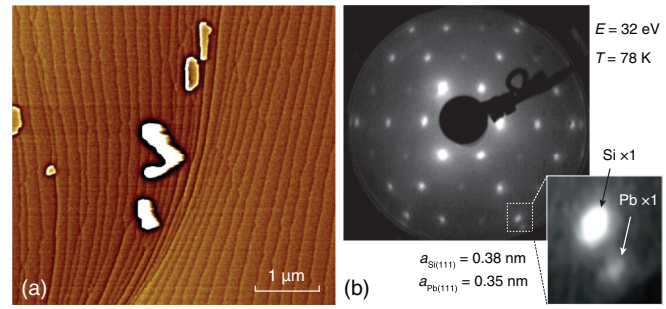

FIG. 4. (a) Large-scale (5×5 μm^2) STM image demonstrating the presence of the bulk Pb islands on the Pb/Mg/Si(111) : B-3 × 3 surface. (b) LEED pattern ($E_p = 32$ eV) from this surface taken at 78 K. The inset shows the enlarged area around the main 1 × 1-Si reflection, where the additional reflection corresponding to the 1 × 1-Pb appears.

It was found that all configurations with Mg beneath the Pb layer are energetically preferable compared to those with Mg atop the Pb layer, which implies penetration of the adsorbed Mg atoms beneath the Pb layer. It is worth noting that Mg intercalation beneath the metal atomic layers on the Si substrate might be a general trend, as it has already been detected for the In/Si(111) [35], Tl/Si(111) [36] and Pb/Si(111) [37] systems.

The most stable Pb/Mg/Si(111):B configuration was found to adopt 1.33 ML of Pb (12 Pb atoms per 3 × 3 unit cell) (Fig. 3). Recall that the 1.33 ML Pb coverage coincides with that of the ideal Pb/Si(111)$\sqrt{3} \times \sqrt{3}$ phase [in reality, the densest striped incommensurate SIC-Pb phase on Si(111) incorporates less Pb coverage, 1.28–1.30 ML of Pb [13,51,52], which is close to the atomic density in the bulk Pb attributed to the Si(111) surface lattice. It should also be noted that 1.33 ML of Pb is noticeably less than 2.0 ML of Pb adopted initially by the plumbene layer before Mg adsorption. Due to the relatively low temperature at which Mg interacts with the Pb layer, Pb desorption can be excluded, and the most plausible scenario is agglomeration of the excess Pb into the 3D islands. In fact, in the STM images at a scale of several micrometers, islands that have a height of several nanometers can be found, which are typically bounded to the step bunches [Fig. 4(a)]. These islands also manifest themselves by the appearance of the satellite LEED spots, which correspond to the lattice constant of the bulk Pb, 0.356 nm [Fig. 4(b)].

Structural model of the Pb/Mg/Si(111) : B-3 × 3 system incorporating 12 Pb atoms and 3 Mg atoms per 3 × 3 unit cell (in the top and side views) is presented in Fig. 2(c), where Pb atoms are shown by the blue balls, Mg atoms by the yellow balls, B atoms by the red balls, and Si atoms by the gray balls. One can see that upon adsorption, Mg atoms penetrate beneath the Pb layer and form there atomic chains with interchain spacing of $3a$ and $1a$ periodicity along the chain. The capping Pb layer is corrugated, namely, the Pb atoms in the vicinity of the Mg atomic chains are pushed up, and the Pb layer also has the basic 3 × 1 periodicity, like that of the array of Mg chains. All of the pushed-up Pb atoms have almost the same height along the chain, but in the experimental STM images, every third Pb atom looks brighter than the others. The simulated STM images (which fairly well reproduce the experimental images) [Fig. 2(d) and Fig. 1SM in the Supplementary Material [53]] disclose this puzzle showing that the bright Pb atom is that having a B atom beneath. Hence, the observed relatively weak STM contrast has an electronic origin, and the resultant 3 × 3 periodicity of the surface is essentially the result of the superposition of the 3 × 1 and $\sqrt{3} \times \sqrt{3}$ lattices of the layer and substrate, respectively.

B. Transport properties

Experimental temperature dependencies of the sheet resistance of the bare Si(111)$\sqrt{3} \times \sqrt{3}$-B sample, Si(111)$\sqrt{3} \times \sqrt{3}$-B sample with plumbene layer grown atop, and Pb/Mg/Si(111) : B-3 × 3 sample are presented in Fig. 5. Note that in the transport measurements we used only the Si(111)substrates with 20–100 Ohm cm resistivity, on which the Si(111)$\sqrt{3} \times \sqrt{3}$-B reconstruction was produced using decomposition of B_2O_3. One can see that the bare Si(111)$\sqrt{3} \times \sqrt{3}$-B sample shows the dependence typical for the metal. Upon application of magnetic field, the resistance slightly increases plausibly due to the weak antilocalization (WAL) effect. The sample with the overgrown plumbene layer demonstrates a very similar behavior regarding the absolute value of resistance, its temperature dependence, and response to the applied magnetic field. The Pb/Mg/Si(111) : B-3 × 3 sample exhibits resistance of the same order of magnitude as those of the above-mentioned samples, albeit lower by ∼13%. The specific feature of its temperature dependence is an abrupt drop at around 6 K, which decreases the sample resistance by ∼5%. Towards the lower temperatures, the resistance shows a sloping growth, which can be attributed to the WAL effect. The resistance drop is naturally explained by the superconducting transition that occurs in the Pb islands into which the Pb atoms liberated upon transition of the plumbene to the 3 × 3-(Pb, Mg) layer agglomerate. The observed transition temperature $T_c \sim 6$ K is slightly lower than the bulk value $T_c = 7.2$ K, which agrees with the data reported earlier for

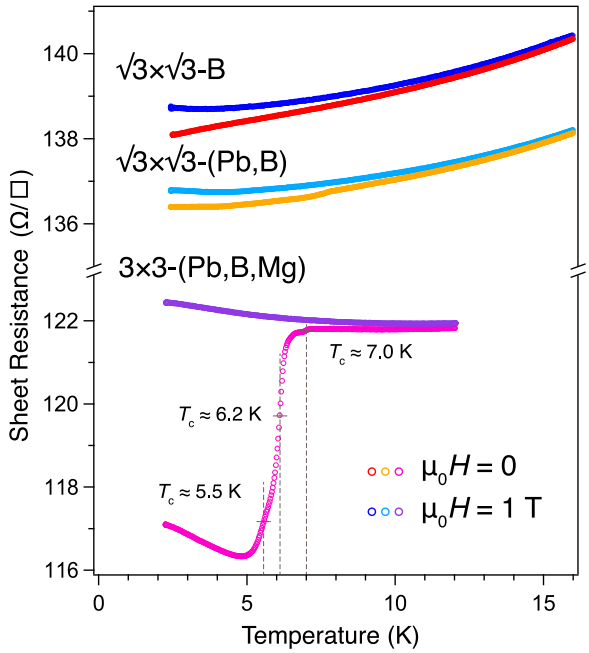

FIG. 5. Temperature dependencies of the sheet resistance of the bare Si(111)$\sqrt{3} \times \sqrt{3}$-B sample, the Si(111)$\sqrt{3} \times \sqrt{3}$-B sample with plumbene layer grown atop, and the Pb/Mg/Si(111) : B-3 × 3 sample measured without and with magnetic field applied perpendicular to the sample surface. For symbol meaning, see the legend.

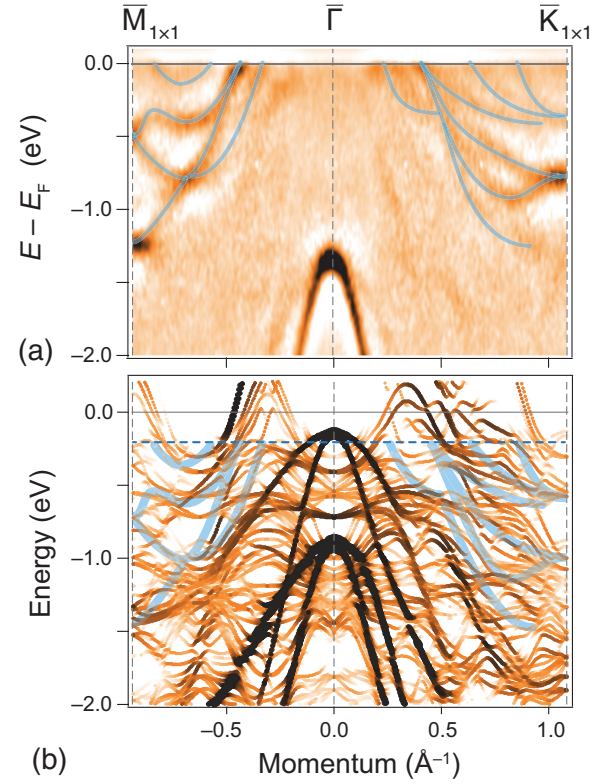

FIG. 6. (a) ARPES spectra for Pb/Mg/Si(111) : B-3 × 3 system recorded within 1 × 1 SBZ. (b) Calculated electronic band structure unfolded into the 1 × 1 SBZ to facilitate comparison with the ARPES data. Horizontal dashed blue line in (b) indicates the position of the experimental Fermi level. The common spectral features in (a) and (b) are marked by the light blue lines to guide the eye.

thin Pb films. Moreover, the critical temperature in thin Pb films is reported to vary with film thickness [54–56] and in the case of Pb islands the superconducting properties depend also on the island size [57–59]. The forming Pb islands vary in size and thickness, which leads to the occurrence of several steps at the resistance drop (Fig. 5). Upon application of the magnetic field, the superconductivity is naturally suppressed, as also demonstrated by Fig. 5.

C. Electronic properties

Figure 6(a) shows the experimental ARPES spectrum from the Pb/Mg/Si(111) : B-3 × 3 sample. Figure 6(b) presents the spectrum calculated on the basis of the structural model shown in Fig. 2(c) and unfolded into the 1 × 1 surface Brillouin zone (SBZ). It is worth noting that their direct comparison is not straightforward. Since the Pb/Mg/Si(111) : B-3 × 3 structure occurs in three domain orientations, the spectrum displays the sum of their contributions. It appears that the ARPES spectrum does not clearly reflect the ×3a periodicity of the system within the 1 × 1 SBZ. Hence, the results of the calculations for each of the three 3 × 3 domains were unfolded onto the 1 × 1 SBZ and then summarized. Nevertheless, in spite of the complicated procedure that generates many zones, one can see a general consistency and find counterparts of the principal ARPES features in the calculated spectrum and *vice versa*. However, ARPES data do not provide sufficient solid ground for the comprehensive assessment of the electronic properties of the various Pb layers with emphasis on their dependence on the layer atomic structure and hosting substrates, especially for the hypothetical cases, like that of the free-standing plumbene. Therefore, we will consider further the results of the DFT calculations, based on the adopted structural model of the Pb layers.

1. Si(111)$\sqrt{3} \times \sqrt{3}$-B *substrate*

As a starting point, consider first the electronic band structure of the basic hosting Si(111)$\sqrt{3} \times \sqrt{3}$-B substrates, both of the "ideal" one with exactly 1/3 ML of B confined in the top Si bilayer and of the "real" Si(111):B sample which contains additional B atoms in the deeper Si bilayer [see Figs. 2SM (a) and (d) in the Supplementary Material [53]]. The inevitable presence of B atoms in the subsurface layers is associated with the high-temperature treatments used during the segregation of B from the sample bulk and B_2O_3 decomposition at the sample surface. In agreement with recently reported results [60,61], our calculations for the "ideal" Si(111)$\sqrt{3} \times \sqrt{3}$-B substrate revealed that it shows up as a semiconductor [Fig. 7(a)], where B-induced bands merge within the Si bulk states area. To explore the effect of subsurface boron on the electronic properties of the Si(111)$\sqrt{3} \times \sqrt{3}$-B sample, we additionally substituted the Si atom for the B atom in the second Si bilayer. Although this simplified structure model does not seem to reproduce the depth distribution of B atoms in the real sample, we believe that it could provide general information on the electronic properties of the sample. One can see that the main effect of adding the subsurface B atom resides in a significant shift of the

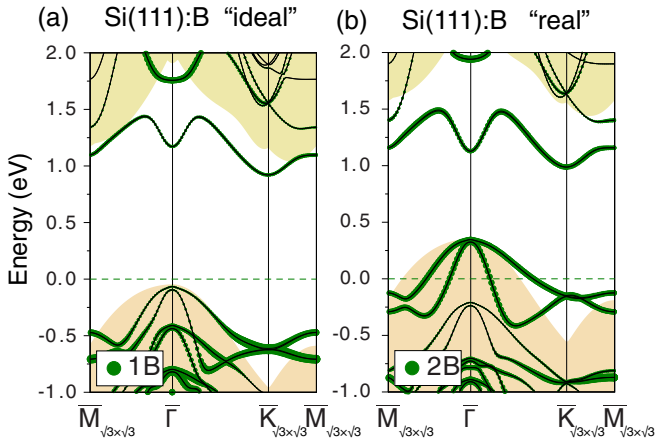

FIG. 7. Relativistic electronic spectra of (a) "ideal" and (b) "real" Si(111):B substrates presented in the $\sqrt{3} \times \sqrt{3}$ SBZ.

Fermi level downwards along the energy scale due to the *p*-doping of the sample [Fig. 7(b)]. As a result, the bands, which were previously laid below the Fermi level, now cross the Fermi level together with the bulk bands, and the sample becomes a metal in agreement with the result of the transport measurements (Fig. 5).

2. *Free-standing plumbene*

At the next step, let us consider the band structure of the free-standing plumbene layer. It is worth noting that plumbenes, depending on the buckling type, demonstrate different electronic properties. The low-buckled plumbene ($\Delta = 1.0$ Å) is predicted to be a trivial insulator [Fig. 8(a)], although under electron doping conditions it can become a topological insulator with a large bulk gap (∼200 meV) [25]. The high-buckled plumbene ($\Delta = 2.65$ Å) demonstrates a metallic band structure [Fig. 8(b)], in agreement with the published

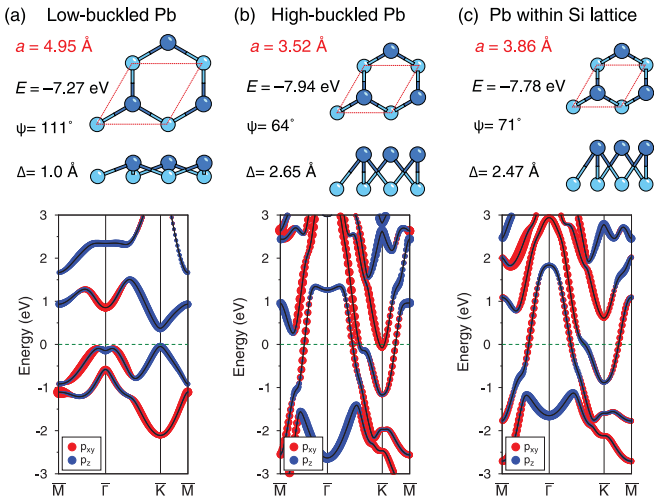

FIG. 8. Orbital-resolved electronic band structure of the free-standing plumbenes: (a) low-buckled, (b) high-buckled, (c) confined into the Si lattice. For each phase, the following structural characteristics are provided: lattice constant a (Å), formation energy E (eV), buckling angle ψ (deg), and buckling height Δ (Å).

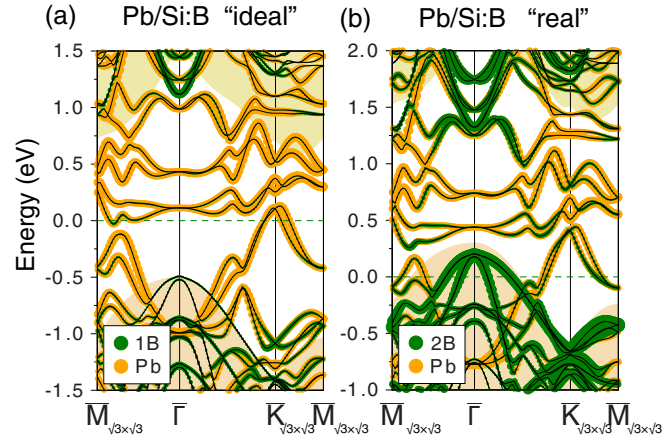

FIG. 9. Element-resolved relativistic electronic spectra of plumbene monolayers on (a) "ideal" and (b) "real" Si(111):B substrates presented in the $\sqrt{3} \times \sqrt{3}$ SBZ. The B- and Pb-originated bands are indicated by green and orange, respectively.

results [24,34]. Interestingly, the free-standing plumbene layer confined to the Si(111) lattice constant ($a = 3.86$ Å) falls into the category of high-buckled plumbenes ($\Delta = 2.47$ Å) and demonstrates an electronic band structure [Fig. 8(c)] very similar to that of the equilibrium high-buckled phase ($a = 3.52$ Å) [Fig. 8(b)]. In particular, one can see in Fig. 8(c) the two highly-dispersing metallic bands formed by the mixture of Pb p_{xy} and p_z orbitals, forming $\overline{\Gamma}$-centered and $\overline{\mathrm{K}}$-centered hole and electron pockets, respectively. According to the formation energy, the plumbene confined to the silicon lattice is only 0.16 eV less stable than the equilibrium high-buckled phase, while the low-buckled phase shows a much larger disfavor in energy (by 0.67 eV).

3. *Plumbene on* Si(111)$\sqrt{3} \times \sqrt{3}$-B

Let us now examine the behavior of the plumbene layer in the presence of a substrate. Figures 9(a) and 9(b) show the elements-resolved relativistic electronic spectra calculated for the plumbene layers placed onto the "ideal" and "real" Si(111):B substrates, respectively [see Figs. 2SM (b) and (e) in the Supplementary Material [53]]. As reported in Ref. [30], the latter case demonstrates a better resemblance with the experimental ARPES spectrum. The distinctive feature of its band structure is a bunch of multiple spin-split Pb-induced bands (shown by orange) dispersing within the silicon bulk gap and intersecting the Fermi level, which stays almost in the middle of the Si band gap [Fig. 9(a)]. In the case of a "real" substrate, the dispersion of the plumbene bands has generally almost the same character; however, the position of the Fermi level is significantly changed: it moves down to the Si valence band area [Fig. 9(b)]. As a result, the Fermi surface is formed not only by the plumbene bands but also to a great extent by the silicon bulk states. Consequently, the transport measurements made before and after plumbene growth on the "real" Si(111)$\sqrt{3} \times \sqrt{3}$-B substrate reveal that the conductance of the system remains essentially unchanged (Fig. 5). Hence, one can conclude that the strong interaction of the plumbene bands with the bulk bands of the "real"

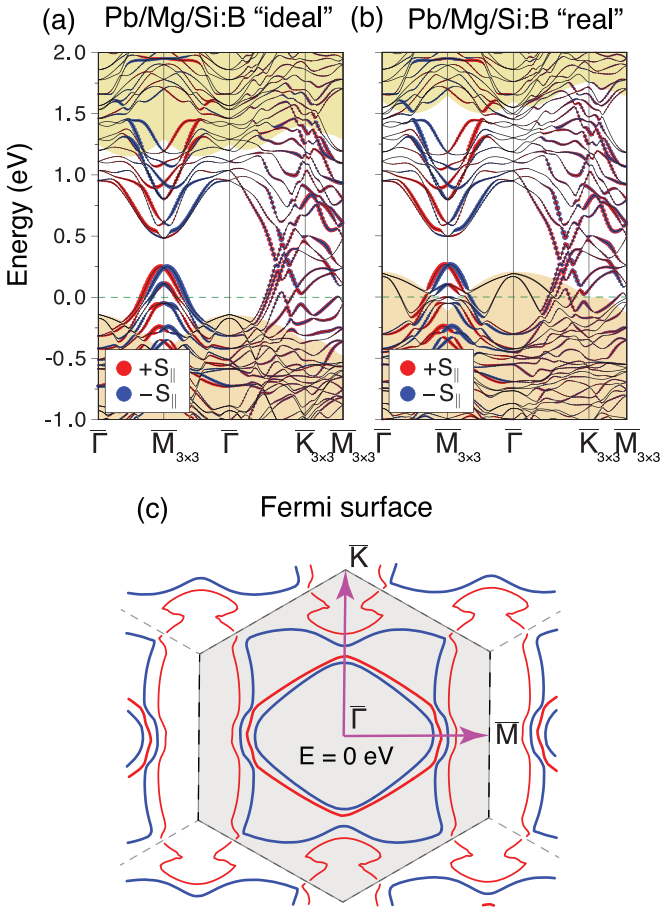

FIG. 10. Spin-resolved relativistic electronic spectra of (Pb, Mg)-3 × 3 layers on (a) "ideal" and (b) "real" Si(111):B substrates presented within the 3 × 3 SBZ. (c) Fermi mapping calculated for the "ideal" system. Red and blue in the electronic spectra and Fermi map represent opposite in-plane and out-of-plane components of the spin expectation values, respectively, while the ball's size reflects the magnitude of the spins. The highlighted hexagon denotes the first 3 × 3 SBZ.

Si(111)$\sqrt{3} \times \sqrt{3}$-B substrate hampers the intrinsic electronic properties of the plumbene layer.

4. Pb/Mg/Si(111) : B-3 × 3 *atomic sandwich*

Motivated by the recently reported finding that intercalation of Mg atoms between the double-layer $\sqrt{7} \times \sqrt{3}$-In phase and Si(111) substrate produces a nearly free-standing double-layer In metal [35], we employed the same approach to the plumbene layer on Si(111)$\sqrt{3} \times \sqrt{3}$-B. However, in contrast to the In double layer, which preserves its entity upon Mg intercalation, the plumbene does not survive. As shown in the previous section, Mg intercalation reduces the Pb coverage in the layer from 2.0 ML to 1.33 ML and changes essentially the layer structure.

Figures 10(a) and 10(b) present the electronic band structures for the Pb/Mg-3 × 3 layers on the "ideal" and "real" Si(111):B substrates, respectively [see Figs. 2SM (c) and (f) in the Supplementary Material [53]], calculated within the first 3 × 3 SBZ. Figure 10(c) shows the Fermi surface map in the case of the "ideal" Pb/Mg/Si(111):B system. One can see that the Fermi surface has an anisotropic shape with certain indications of the quasi-one-dimensional features, which stem from the stripe-like atomic arrangement of the Pb-Mg layers in real space.

When addressing the "real" Pb/Mg/Si(111) : B-3 × 3 system (Fig. 10), one can see that adding subsurface boron does not greatly affect the shape of the surface-state bands and results only in a shifting Fermi level together with all surface-state bands downwards into the region of bulk valence band. As in all the above-mentioned cases, the conductance of the sample Pb/Mg/Si(111): B is mainly associated with the bulk contribution, and all samples display very similar resistance values (Fig. 5).

IV. SUMMARY

In summary, we explore the structure and electronic properties of a plumbene layer grown on the Si(111)$\sqrt{3} \times \sqrt{3}$-B surface and its modification caused by Mg adsorption, using LEED and STM observations, as well as DFT calculations. In particular, it was found that Mg adsorbed onto the grown plumbene intercalates between the Pb layer and the Si(111)$\sqrt{3} \times \sqrt{3}$-B substrate to form the Pb/Mg/Si(111):B atomic sandwich. The change in the interface structure affects the Pb overlayer, which changes from a bilayer having the high-buckled plumbene structure to a single-atom layer containing 1.33 ML of Pb, as revealed by DFT-AIRSS analysis, arranged in a stripelike structure, which together with the substrate adopts the overall 3 × 3 periodicity. The electronic properties of the Pb/Si(111):B and Pb/Mg/Si(111):B systems were systematically explored using DFT calculations for the Si(111)$\sqrt{3} \times \sqrt{3}$-B substrate with 1/3 ML B only in the top Si bilayer (denoted as "ideal" substrate) and the Si(111)$\sqrt{3} \times \sqrt{3}$-B substrate with added subsurface B doping (denoted as "real" substrate). The presence of B atoms in the subsurface layers is associated with the high-temperature treatments employed both during B segregation from the sample bulk and B_2O_3 decomposition at the sample surface for the Si(111)$\sqrt{3} \times \sqrt{3}$-B formation. It appears that intrinsic properties of the Pb layers are overshadowed by electronic properties of the real Si(111):B substrate, which underwent a strong subsurface *p*-type doping. The dominated contribution of the substrate bands to the electronic properties of the system was confirmed in the *in situ* low-temperature transport measurements, which showed that the Si(111)$\sqrt{3} \times \sqrt{3}$-B substrate with and without plumbene, as well as Pb/Mg/Si(111):B samples, display very similar sheet resistance values. The obtained results reveal that utilization of the unique electronic properties of the low-dimensional structures (e.g., 2D Xenes, in particular, plumbene) requires a solution of the complex problem: It is not enough to find a proper substrate to support the low-dimensional structure, but it is also necessary that this structure would provide a dominant contribution to the electronic properties of the formed material system.

ACKNOWLEDGMENTS

The work was supported by the Russian Science Foundation (Grant No. 22-12-00174 [62]). Transport measurements

were supported by the Government research assignment for IACP FEB RAS, Project FWFW-2021-0002. The calculations were conducted using the equipment of Shared Resource Center Far Eastern Computing Resource IACP FEB RAS [63].

DATA AVAILABILITY

No data were created or analyzed in this study.

[1] M. Yakes, M. Hupalo, M. A. Zaluska-Kotur, Z. W. Gortel, and M. C. Tringides, Low-temperature ultrafast mobility in systems with long-range repulsive interactions: Pb/Si(111), Phys. Rev. Lett. **98**, 135504 (2007).

[2] M. Hupalo and M. C. Tringides, Ultrafast kinetics in Pb/Si(111) from the collective spreading of the wetting layer, Phys. Rev. B **75**, 235443 (2007).

[3] K. L. Man, M. C. Tringides, M. M. T. Loy, and M. S. Altman, Anomalous mass transport in the Pb wetting layer on the Si(111) surface, Phys. Rev. Lett. **101**, 226102 (2008).

[4] A. V. Matetskiy, L. V. Bondarenko, D. V. Gruznev, A. V. Zotov, A. A. Saranin, and M. C. Tringides, Structural transformations in Pb/Si(111) phases induced by C_{60} adsorption, J. Phys.: Condens. Matter **25**, 395006 (2013).

[5] E. Granato, S. C. Ying, K. R. Elder, and T. Ala-Nissila, Anomalous fast dynamics of adsorbate overlayers near an incommensurate structural transition, Phys. Rev. Lett. **111**, 126102 (2013).

[6] K. Yaji, Y. Ohtsubo, S. Hatta, H. Okuyama, K. Miyamoto, T. Okuda, A. Kimura, H. Namatame, M. Taniguchi, and T. Aruga, Large Rashba spin splitting of a metallic surface-state band on a semiconductor surface, Nat. Commun. **1**, 17 (2010).

[7] K. Yaji, S. Hatta, T. Aruga, and H. Okuyama, Structural and electronic properties of the Pb/Ge(111)-$\beta(\sqrt{3}\times\sqrt{3})R30^\circ$ surface studied by PES and first-principles calculations, Phys. Rev. B **86**, 235317 (2012).

[8] M. Szary, Role of coupling between surface orbitals in soc enhanced spin splitting, Surf. Sci. **684**, 12 (2019).

[9] T. Zhang, P. Cheng, W. J. Li, Y. J. Sun, G. Wang, X. G. Zhu, K. He, L. Wang, X. Ma, X. Chen, Y. Wang, Y. Liu, H. Q. Lin, J. F. Jia, and Q. K. Xue, Superconductivity in one-atomic-layer metal films grown on Si(111), Nat. Phys. **6**, 104 (2010).

[10] M. Yamada, T. Hirahara, and S. Hasegawa, Magnetoresistance measurements of a superconducting surface state of In-induced and Pb-induced structures on Si(111), Phys. Rev. Lett. **110**, 237001 (2013).

[11] A. Stępniak, A. L. Vanegas, M. Caminale, H. Oka, D. Sander, and J. Kirschner, Atomic layer superconductivity, Surf. Interface Anal. **46**, 1262 (2014).

[12] J. Noffsinger and M. L. Cohen, Superconductivity in monolayer Pb on Si(111) from first principles, Solid State Commun. **151**, 421 (2011).

[13] C. Brun, T. Cren, V. Cherkez, F. Debontridder, S. Pons, D. Fokin, M. C. Tringides, S. Bozhko, L. B. Ioffe, B. L. Altshuler, and D. Roditchev, Remarkable effects of disorder on superconductivity of single atomic layers of lead on silicon, Nat. Phys. **10**, 444 (2014).

[14] M. Ligges, M. Sandhofer, I. Sklyadneva, R. Heid, K. P. Bohnen, S. Freutel, L. Retting, P. Zhou, P. M. Echenique, E. V. Chulkov, and U. Bovensiepen, Electron-phonon coupling in quantum-well states of the Pb/Si(111) system, J. Phys.: Condens. Matter **26**, 352001 (2014).

[15] F. Oguro, Y. Sato, K. Asakawa, M. Haze, and Y. Hasegawa, Enhanced critical magnetic field for monatomic-layer superconductor by Josephson junction steps, Phys. Rev. B **103**, 085416 (2021).

[16] C. Brun, T. Cren, and D. Roditchev, Review of 2D superconductivity: the ultimate case of epitaxial monolayers, Supercond. Sci. Technol. **30**, 013003 (2017).

[17] Y. Sato, M. Haze, R. Nemoto, W. Qian, S. Yoshizawa, T. Uchihashi, and Y. Hasegawa, Squeezed Abrikosov-Josephson vortex in atomic-layer Pb superconductors formed on vicinal Si(111) substrate, Phys. Rev. Lett. **130**, 106002 (2023).

[18] L. V. Bondarenko, A. Y. Tupchaya, Y. E. Vekovshinin, D. V. Gruznev, T. V. Utas, A. N. Mihalyuk, N. V. Denisov, A. V. Zotov, and A. A. Saranin, Dense single-atomic $14\times\sqrt{3}$-reconstructed Pb layer on Si(111): Structural and superconducting properties, Phys. Rev. B **108**, 115428 (2023).

[19] J. Yuhara and G. Le Lay, Beyond silicene: synthesis of germanene, stanene and plumbene, Jpn. J. Appl. Phys. **59**, SN0801 (2020).

[20] K. A. Lozovoy, I. I. Izhnin, A. P. Kokhanenko, V. V. Dirko, V. P. Vinarskiy, A. V. Voitsekhovskii, O. I. Fitsych, and N. Y. Akimenko, Single-element 2D materials beyond graphene: Methods of epitaxial synthesis, Nanomaterials **12**, 2221 (2022).

[21] J. Chen, C. Wabg, H. Li, X. Xu, J. Yang, Z. Huo, L. Wang, W. Zhang, X. Xiao, and Y. Ma, Recent advances in surface modifications of elemental two-dimensional materials: Structure, properties, and applications, Molecules **28**, 200 (2023).

[22] C. Grazianetti, A. Molle, and C. Martella, The future of xenes beyond graphene: challenges and perspective, 2D Mater. **11**, 042005 (2024).

[23] Z. Q. Huang, C. H. Hsu, F. C. Chuang, Y. T. Liu, H. Lin, W. S. Su, V. Ozolins, and A. Bansil, Strain driven topological phase transitions in atomically thin films of group IV and V elements in the honeycomb structures, New J. Phys. **16**, 105018 (2014).

[24] P. Rivero, J.-A. Yan, V. M. García-Suárez, J. Ferrer, and S. Baraza-Lopez, Stability and properties of high-buckled two-dimensional tin and lead, Phys. Rev. B **90**, 241408(R) (2014).

[25] X. L. Yu, L. Huang, and J. Wu, From a normal insulator to a topological insulator in plumbene, Phys. Rev. B **95**, 125113 (2017).

[26] D. K. Das, J. Sarkar, and S. K. Singh, Effects of sample size, temperature and strain velocity on mechanical properties of plumbene by tensile loading along longitudinal direction: A molecular dynamics study, Comput. Mater. Sci. **151**, 196 (2018).

[27] X. L. Yu and J. Wu, Evolution of topological properies of two-dimensional group iva materials and device design, Phys. Chem. Chem. Phys. **20**, 2296 (2018).

[28] J. Yuhara, B. He, N. Matsunami, M. Nakata, and G. Le Lay, Graphene's latest cousin: Plumbene epitaxial growth on a "nano watercube", Adv. Mater. **31**, 1901017 (2019).

[29] G. Bihlmayer, J. Sassmannshausen, A. Kubetzka, S. Blügel, K. von Bergmann, and R. Wiesendanger, Plumbene on a magnetic substrate: A combined scanning tunneling microscopy and density functional theory study, Phys. Rev. Lett. **124**, 126401 (2020).

[30] D. V. Gruznev, L. V. Bondarenko, A. Y. Tupchaya, A. A. Yakovlev, A. V. Slyshkin, A. N. Mihalyuk, A. V. Zotov, and A. A. Saranin, Formation of a double-layer Pb reconstruction on the B-segregated Si(111) surface, Surf. Sci. **706**, 121784 (2021).

[31] D. K. Das and B. Kumar, Plumbene a promising material for future technology: A review, Comput. Mater. Sci. **247**, 113487 (2025).

[32] H. Kim, Y. Miyata, and Y. Hasegawa, Superconducting proximity effect on a Rashba-split Pb/Ge(111)-$\beta\sqrt{3}\times\sqrt{3}$ surface, Supercond. Sci. Technol. **29**, 084006 (2016).

[33] H. Huang, H. Toyama, L. Bondarenko, A. Tupchaya, D. V. Gruznev, A. Takayama, R. Hobara, R. Akiyama, A. V. Zotov, A. A. Saranin, and S. Hasegawa, Superconducting proximity effect in a Rashba-type surface state of Pb/Ge(111), Supercond. Sci. Technol. **33**, 075007 (2020).

[34] B. Zhang, F. Guo, M. Zhu, L. Feng, and Y. Zheng, The sensitive tunability of superconducting critical temperature in high-buckled plumbene by shifting Fermi level, Physica E **130**, 114688 (2021).

[35] S. Terakawa, S. Hatta, H. Okuyama, and T. Aruga, Ultrathin (In, Mg) films on Si(111): A nearly freestanding double-layer metal, Phys. Rev. B **105**, 125402 (2022).

[36] A. Y. Tupchaya, L. V. Bondarenko, Y. E. Vekovshinin, A. A. Yakovlev, A. N. Mihalyuk, D. V. Gruznev, C. R. Hsing, C. M. Wei, A. V. Zotov, and A. A. Saranin, Double-atomic-layer Tl-Mg compound on a Si(111) surface with advanced electronic properties, Phys. Rev. B **101**, 235444 (2020).

[37] A. Y. Tupchaya, L. V. Bondarenko, A. A. Yakovlev, Y. E. Vekovshinin, A. N. Mihalyuk, D. V. Gruznev, N. S. Denisov, A. V. Matetskiy, A. Y. Aladyshkin, A. V. Zotov, and A. A. Saranin, 2D system incorporating perforated Mg sheet sandwiched between Pb layer and Si(111), Appl. Surf. Sci. **589**, 152951 (2022).

[38] G. Kresse and J. Hafner, *Ab initio* molecular dynamics for liquid metals, Phys. Rev. B **47**, 558 (1993).

[39] G. Kresse and D. Joubert, From ultrasoft pseudopotentials to the projector augmented-wave method, Phys. Rev. B **59**, 1758 (1999).

[40] P. E. Blöchl, Projector augmented-wave method, Phys. Rev. B **50**, 17953 (1994).

[41] J. P. Perdew, K. Burke, and M. Ernzerhof, Generalized gradient approximation made simple, Phys. Rev. Lett. **77**, 3865 (1996).

[42] L. G. Ferreira, M. Marques, and L. K. Teles, Approximation to density functional theory for the calculation of band gaps of semiconductors, Phys. Rev. B **78**, 125116 (2008).

[43] L. G. Ferreira, M. Marques, and L. K. Teles, Slater half-occupation technique revisited: the LDA-1/2 and GGA-1/2 approaches for atomic ionization energies and band gaps in semiconductors, AIP Adv. **1**, 032119 (2011).

[44] C. J. Pickard and R. J. Needs, *Ab initio* random structure searching, J. Phys.: Condens. Matter **23**, 053201 (2011).

[45] C. J. Pickard, Ephemeral data derived potentials for random structure search, Phys. Rev. B **106**, 014102 (2022).

[46] J. Tersoff and D. R. Hamann, Theory of the scanning tunneling microscope, Phys. Rev. B **31**, 805 (1985).

[47] R. L. Headrick, I. K. Robinson, E. Vlieg, and L. C. Feldman, Structure determination of Si(111):B($\sqrt{3}\times\sqrt{3}$)*R*30 surface. subsurface substitutional doping, Phys. Rev. Lett. **63**, 1253 (1989).

[48] I. W. Lyo, E. Kaxiras, and P. Avouris, Adsorption of boron on Si(111): Its effect on surface electronic states and reconstruction, Phys. Rev. Lett. **63**, 1261 (1989).

[49] P. J. Bedrossian, R. D. Meade, K. Mortensen, D. M. Chen, J. A. Golovchenko, and D. Vanderbilt, Surface doping and stabilization of Si(111) with boron, Phys. Rev. Lett. **63**, 1257 (1989).

[50] F. Bechstedt, *Principles of Surface Physics*, 1st ed., Advanced Texts in Physics (Springer-Verlag, Berlin, 2003).

[51] S. Stepanovsky, M. Yakes, V. Yeh, M. Hupalo, and M. C. Tringides, The dense α-$\sqrt{3}\times\sqrt{3}$Pb/Si(111) phase: A comprehensive STM and SPA-LEED study of ordering, phase transitions and interactions, Surf. Sci. **600**, 1417 (2006).

[52] C. Brand, S. Muff, M. Fanciulli, H. Pfnür, M. C. Tringides, J. H. Dil, and C. Tegenkamp, Spin-resolved band structure of a densely packed Pb monolayer on Si(111), Phys. Rev. B **96**, 035432 (2017).

[53] See Supplemental Material at http://link.aps.org/supplemental/10.1103/PhysRevB.111.125401 for additional figures.

[54] Y. Guo, Y. F. Zhang, X. Y. Bao, T. Z. Han, Z. Tang, L. X. Zhang, W. G. Zhu, E. G. Wang, Q. Niu, Z. Q. Qiu, J. F. Jia, Z. X. Zhao, and Q. K. Xue, Superconductivity modulateded by quantum size effects, Science **306**, 1915 (2004).

[55] S. Qin, J. Kim, Q. Niu, and C. K. Shih, Superconductivity at the two-dimensional limit, Science **324**, 1314 (2009).

[56] W. Zhao, Q. Wang, M. Liu, W. Zhang, Y. Wang, M. Chen, Y. Guo, K. He, X. Chen, Y. Wang, J. Wang, X. Xie, Q. Niu, L. Wang, X. Ma, J. K. Jain *et al.*, Evidence for Berezinskii-Kosterlitz-Touless transition in atomically flat two-dimensional Pb superconducting films, Solid State Commun. **165**, 59 (2013).

[57] D. Eom, S. Qin, M. Y. Chou, and C. K. Shih, Persistent superconductivity in ultrathin Pb films: A scanning tunneling spectroscopy study, Phys. Rev. Lett. **96**, 027005 (2006).

[58] T. Nishio, T. An, A. Nomura, K. Miyachi, T. Eguchi, H. Sakata, S. Lin, N. Hayashi, N. Nakai, M. Machida, and Y. Hasegawa, Superconducting Pb island nanostructures studied by scanning tunneling microscopy and spectroscopy, Phys. Rev. Lett. **101**, 167001 (2008).

[59] J. Liu, X. Wu, F. Ming, X. Zhang, K. Wang, B. Wang, and X. Xiao, Size-dependent superconducting state of individual nanosized Pb islands grown on Si(111) by tunneling spectroscopy, J. Phys.: Condens. Matter **23**, 265007 (2011).

[60] H. Q. Shi, M. W. Radny, and P. V. Smith, Electronic structure of the Si(111)$\sqrt{3}\times\sqrt{3}R30^\circ$-B surface, Phys. Rev. B **66**, 085329 (2002).

[61] H. Aldahhak, C. Hogan, S. Lindner, S. Appelfeller, H. Eisele, W. G. Schmidt, M. Dähne, U. Gerstmann, and M. Franz, Electronic structure of the Si(111)$\sqrt{3}\times\sqrt{3}R30^\circ$-B surface from theory and photoemission spectroscopy, Phys. Rev. B **103**, 035303 (2021).

[62] https://rscf.ru/en/project/22-12-00174/.

[63] https://cc.dvo.ru.